Hindawi Publishing Corporation
International Journal of Photoenergy
Volume 2016, Article ID 2736257, 9 pages
http://dx.doi.org/10.1155/2016/2736257

Research Article

Ag-Doped TiO_2 Nanotube Arrays Composite Film as a Photoanode for Enhancing the Photoelectric Conversion Efficiency in DSSCs

Jinghua Hu,[1,2] Jiejie Cheng,[1] Shengqiang Tong,[1] Yingping Yang,[1,3] Mengwei Chen,[1] and Shiwu Hu[1]

[1]*School of Science, Wuhan University of Technology, Wuhan 430070, China*
[2]*Department of Chemical and Petroleum Engineering, The University of Pittsburgh, Pittsburgh, PA 15261, USA*
[3]*Department of Electrical and Computer Engineering, University of North Carolina at Charlotte, Charlotte, NC 28223, USA*

Correspondence should be addressed to Yingping Yang; ypyang@whut.edu.cn

Received 17 June 2016; Accepted 8 August 2016

Academic Editor: Minlin Jiang

A Ag-doped double-layer composite film with TiO_2 nanoparticles (P25) as the underlayer and TiO_2 nanotube (TNT) arrays with the Ag-doped nanoparticles as the overlayer was fabricated as the photoanode in dye-sensitized solar cells (DSSCs). Five different concentrations of Ag-doped TNT arrays photoelectrode were compared with the pure TNT arrays composite photoelectrode. It is found that the photoelectric conversion efficiency of the TNT arrays composite photoanode is gradually improved from 3.00% of the pure TNT arrays composite photoanode to 6.12% of the Ag-doped TNT arrays photoanode with the increasing of the doping concentration, reaching up to the maximum in the 0.04 mol/L $AgNO_3$ solution, and then slightly decreased to 5.43% after continuing to increase the doping concentration. The reason is mainly that the cluster structure of the Ag nanoparticles with large surface area contributes to dye adsorption and the Surface Plasmon Resonance Effect of the Ag nanoparticles improved the photocatalytic ability of the TNT arrays film.

1. Introduction

Dye-sensitized solar cells (DSSCs) have aroused more and more concern because of the following characteristics: simple preparation process, low production cost, environmentally friendly and easily obtained materials, and no geographical restriction in recent decades [1, 2]. In general, DSSCs are composed of a dye-sensitized nanocrystalline TiO_2 film photoanode, the redox electrolyte, and a Pt-coated counter electrode [3]. As for the important part of the DSSCs, the nanocrystalline TiO_2 film photoanode has a great effect on dye adsorption, photon capture, electronic collection, and transmission, which greatly influences the photoelectric conversion efficiency of DSSCs [4]. The TiO_2 nanoparticles films have large specific surface area and small particle size, which greatly enhanced the dye adsorption and the connection between the conduction glass substrate and the TiO_2 nanofilms [5]. Its advantages are widely used in DSSCs. However, such films exhibit poor light absorption ability because of their high transparency in the visible range [6, 7]. What is worse, the multiple trapping/detrapping events occurring in the grain boundaries between three-dimensional networks of interconnected nanoparticles greatly suppressed the electron transport rate [8]. These factors greatly influence the photoelectric conversion efficiency of the DSSCs.

Some researchers have found that the introduction of one-dimensional nanostructures on DSSCs can improve the transmission performance of the electron [9–11]. Then, many kinds of one-dimensional nanomaterials have been synthesized and applied on the DSSCs, such as nanowires [12], nanorods [13, 14], and nanotubes [15, 16]. Their special one-dimensional nanostructures provide direct access to the electronic transmission, leading to the suppressed electron

recombination. Asagoe et al. reported that a high photoelectric conversion efficiency of 6.53% was achieved by mixing the mass ratio of 10% nanowires with P25 nanoparticles of anatase phase [17]. Adachi et al. also demonstrated that titania thin film electrode composed of a network structure of single crystal-like TiO_2 nanowires was applied on the DSSCs and achieved a high light-to-electricity conversion yield of 9.3% [18]. Jiu et al. reported that a highly crystalline TiO_2 nanorod synthesized by a hydrothermal process was designed on the DSSCs and a high photoelectric conversion efficiency of 7.29% was obtained [19]. Hafez et al. issued a report that a novel TiO_2 nanorod/nanoparticles bilayer electrode showed high light-to-energy conversion efficiency of 7.1% [20]. According to the report by Rho and Suh, the energy conversion efficiency of the DSSCs was significantly improved from 5.2% to 6.3% by filling approximately 10 wt% of TiO_2 nanoparticles to the TiO_2 nanotube membranes [21].

Although the introduction of one-dimensional TiO_2 nanostructure can greatly improve the electron transfer rate, the TiO_2 nanomaterial has its own weakness, that is, poor light-harvesting ability and dye adsorption [22]. Studies have shown that some metal nanoparticles can improve the energy level structure of the TiO_2 nanomaterials and enhance the ability of light absorption [23]. Wang et al. found that TiO_2 powder mixed with Er^{3+} showed a higher photocatalytic activity, compared with the pure TiO_2 powder [24]. Wang et al. showed that (Ag,S) modified TiO_2 photoanodes exhibited a strong performance of light absorption in the UV-Vis region and a clear reduction in charge transport resistance [25]. The photoelectric conversion efficiency has been increased by introducing Au or Ag nanoparticles into TiO_2 nanoparticles films on DSSCs [26–28]. Under the light conditions, the free electrons of the metal surface interacted with the photons, caused the Surface Plasmon Resonance Effects, and improved the performance of light-harvesting.

In this work, we report a double-layer TiO_2 composite film photoanode consisting of TiO_2 nanotube (TNT) arrays film as the overlayer and P25 nanoparticles as the underlayer. The underlayer prepared by P25 nanoparticles can improve the dye adsorption, and the TNT arrays overlayer film provides rapid transmission way for electron. In addition, in order to investigate the influence on the photoelectric conversion efficiency of the TiO_2 composite film photoanode, five different concentrations of $AgNO_3$ (0.01 mol/L, 0.02 mol/L, 0.03 mol/L, 0.04 mol/L, and 0.05 mol/L $AgNO_3$ solutions) were mixed into the double-layer TiO_2 composite film photoanode and their photovoltaic performances were compared and analyzed.

2. Experiment

2.1. Preparation of the TNT Arrays Film. TNT arrays films were synthesized by two-step anodization method. The detailed steps of the anodization are shown in Figure 1. As can be seen, Ti foils (2 cm × 2.5 cm, Sigma-Aldrich, 99.7% purity) are served as the positive electrode and the Pt foils are used as the counter electrode by using a DC power source (DYY-6C). The redox reaction was carried out in electrolyte at room temperature under a constant voltage of 40 V. The electrolyte was prepared by the ammonium fluoride (NH_4F, 0.5 wt%), ethylene glycol, and DI water (2 vol%). The first anodization was performed in a reaction tank for 19 h and stirred with magnetic stirrer in the whole reaction process. After the first anodization, the as-anodized Ti substrate was rinsed by the anhydrous ethanol, dried in the air, and then annealed at 450°C for 30 min with a heating rate of 2°C/min to induce crystallinity. The second anodization was performed on the as-anodized Ti substrate under the same conditions for 1 h to form an amorphous TiO_2 layer between the Ti foil and the TNT arrays grown on the surface of the Ti foils. After the anodization, a free-standing TNT array was separated from the Ti substrate.

2.2. Preparation of the P25/TNT Arrays Composite Film Photoanode. The P25 paste was synthesized by grinding with an agate mortar. The quantities of TiO_2 powder and acetic acid were mixed into the mortar and DI water and anhydrous ethanol were added on a regular basis. Then, the grinding TiO_2 powder was added to the terpineol, ethyl cellulose colloid, and anhydrous ethanol and stirred until the anhydrous ethanol evaporated completely. Finally, the P25 paste was obtained and kept at low temperature with a sealing membrane.

For fabrication of the TiO_2 double-layer composite film photoanode, the P25 paste was posted on the FTO glass by doctor-blade technique and the thickness was controlled by the layer numbers of adhesive tape. Then, the prepared TNT arrays film was moved to the P25 paste with a small blade and annealed at 450°C for 30 min with a heating rate of 2°C/min.

2.3. Preparation of the Ag-Doped P25/TNT Arrays Composite Film Photoanode. For formation of the Ag-doped TiO_2 double-layer composite film photoanode, 0.1 mol/L $AgNO_3$ solution was configured and diluted into the corresponding value. Five different concentrations of $AgNO_3$ solutions (0.01 mol/L, 0.02 mol/L 0.03 mol/L, 0.04 mol/L, and 0.05 mol/L) were prepared. By using the characteristics of light decomposition of $AgNO_3$, the P25/TNT arrays composite film photoanode was immersed into different concentration $AgNO_3$ solutions with a UV lamp irradiation for 2 minutes, then rinsed with anhydrous ethanol, and dried. Finally, the Ag nanoparticles were successfully added to the TNT arrays. The schematic of fabrication of the Ag-doped TNT arrays composite film was shown in Figure 2.

2.4. Fabrication of the DSSCs. To fabricate the DSSCs, the Ag-doped and untreated TiO_2 composite film photoanode were immersed into the 0.5 mM ethanol solution of N719 under the dark condition at room temperature for 24 h to complete the sensitizer uptake. The sensitized photoanode was then rinsed with anhydrous ethanol and dried naturally. Finally, the three edges of the photoanode were pasted with transparent adhesive tape and they were assembled into a typical sandwich cell with a Pt-coated FTO conducting glass. A mask with a square hole in the middle (4 mm × 4 mm) was used to control the effective area of the DSSCs.

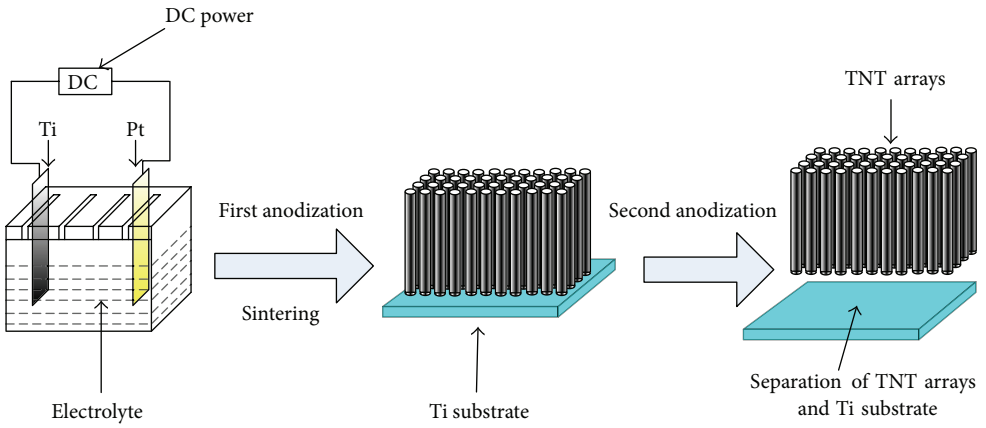

Figure 1: The schematic of the TNT arrays film preparation.

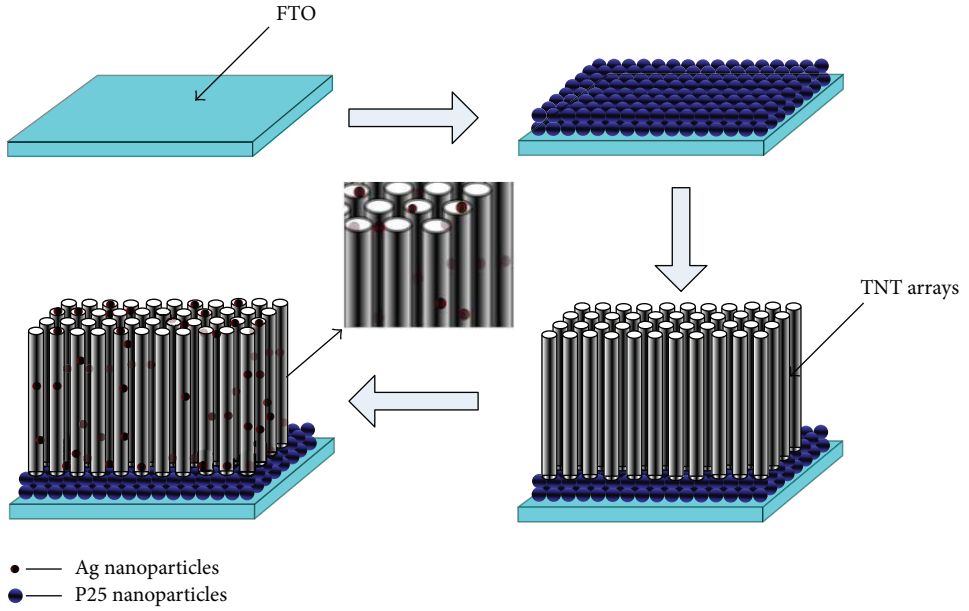

Figure 2: The schematic of fabrication of the Ag-doped TNT arrays composite film.

The electrolytes containing 0.5 M 4-tert-butylpyridine, 0.5 M LiI, 0.05 M I_2, and 0.3 M 1,2-dimethyl-3-propylimidazolium iodide (DMP II) in dry acetonitrile were injected into inner cell at the edge of no tape by the capillary forces. Then, the cell was tested immediately.

2.5. Characterization and Measurement. The crystallinity and the phase-purity of the samples with the Ag-doped and untreated TiO_2 composite film photoanode were performed on a D/MAX-RB/RU-200B Rotation Anode High Power X-Ray Diffractometer (XRD) with Cu Kα radiation (λ = 0.15406 nm). Scanning electron microscopy (SEM) was used to characterize the morphology on a Zeiss Ultra Plus (Germany) field emission SEM. The identification of the internal morphology and the nanocrystal were studied by a JEM2100F (Japan) transmission electron microscopy (TEM). The UV-Vis absorption spectra of the TiO_2 composite film photoanode and the solution of the dye-sensitized TiO_2 composite film photoanode after being desorbed were measured on a UV/Vis-NIR spectrophotometer (UV-3150), and the desorption solution is 0.1 M of the aqueous solution of NaOH.

The current density-voltage (J-V) characteristics curve of the DSSCs was used to explain the photoelectric performance of the cell performed on a CHI640E electrochemical workstation analyzer. The solar light was provided by a solar light simulator (Microsolar 300) under 100 mW/cm^{-2} light illumination condition calibrated with accurate illumination meter.

3. Results and Discussion

3.1. Microstructure and Morphology. Figures 3(a) and 3(b) show the typical SEM images of the top and cross-sectional morphology of the Ag-doped TNT arrays composite film

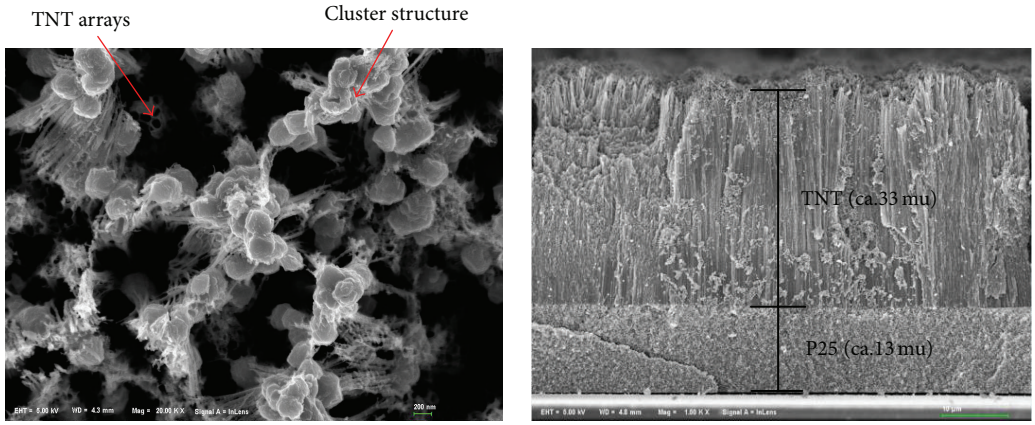

(a) (b)

Figure 3: The typical SEM images of the Ag-doped TNT arrays composite film photoanode after annealing at 450°C for 30 min in the top-view (a) and in cross-sectional view (b).

photoanode after annealing at 450°C for 30 min. It can be seen from Figure 3(a) that a number of Ag nanoparticles that formed the clusters were adsorbed on the TNT arrays. Clusters are composed of a few to thousands of molecules, atoms, or irons through the interactions between physical and chemical force. The Ag nanoparticles on the surface with larger surface area combined into metal clusters by metal bond. Its advantages resulted in more dye adsorption. Some relatively small clusters enter into the tubular structure of the TNT arrays, which can be seen from the TEM images. Figure 3(b) displays that the double-layer composite film consists of the underlayer P25 nanoparticles film (the thickness is 13 μm) and the top-layer TNT arrays film (the thickness is 33 μm). The P25 nanoparticles are combined closely with the FTO conductive glass and the TNT arrays.

Figures 4(a)–4(e) show the TEM image of the different concentration Ag-doped TNT arrays. It can be seen that Ag nanoparticles have been successfully doped into the tubular structure of the TNT arrays or attached to the tube wall. In addition, with the increase of the doping concentration, the Ag nanoparticles of the TNT arrays were detected more and more.

Figure 5(a) displays the TEM images of a single Ag-doped TiO_2 nanotube. A small black particle in the tube can be clearly seen. The energy spectrum was obtained by using electron beam to strike the black particle shown in Figure 5(b). It clearly illustrates that the Ag content is the highest in this point, followed by the Ti and O, which further clarify the existence of Ag nanoparticles. The $AgNO_3$ solution was successfully decomposed into Ag nanoparticles and entered into the TNT arrays or attached on the tube wall.

3.2. Crystal Structure. Figure 6(a) shows the typical XRD pattern of TNT arrays composite film photoanode annealed at 450°C for 30 min. It can be seen that all the diffraction peaks (101), (004), (200), (105), (211), and (204) can be matched with the standard anatase PDF card, which illustrates that the crystallinity of P25 nanoparticles and the crystallinity of the TNT arrays are very high after sintering at 450°C, and all of these are pure anatase phase.

Figure 6(b) displays the XRD pattern of Ag-doped TNT arrays composite film photoanode after being annealed at the same temperature. As we can see some of the diffraction peaks of anatase phase have been enhanced after doping with the Ag nanoparticles. For example, the anatase peaks of (004) and (105) are enhanced greatly, mainly because the single crystal plane (111) of the Ag corresponding to the characteristic peak is relatively close to the characteristic peak of the anatase phase TiO_2 crystal plane (004) so that the characteristic peaks overlap each other and the single crystal plane (006) of the Ag overlaps with the characteristic peak of the anatase phase TiO_2 crystal plane (105) too. In addition, the diffraction peaks (104) and (112) of the Ag single crystal plane are indexed to the standard PDF card. This result indicates that the phase structure of the TNT arrays composite film has not changed after being doped with the Ag nanoparticles, which is still the anatase phase.

3.3. UV-Vis Absorption Spectra Measurements. The amount of dye adsorption and the absorption capacity of light for the photoanode greatly affect the performance of the DSSCs [29]. In order to calculate the amount of dye adsorption on the photoanode according to the Lambert-Beer Law $A = KCL$ (A is the absorbance, K is the molar absorption, C is the concentration of the substance, and L is the thickness of the absorption layer.), the 0.1 M NaOH solution was used to remove the dye molecules from the sensitized photoanode. As shown in Figure 7, it displays that spectral absorption of analytical solution of the pure sensitized TNT arrays is the smallest. With the increase of the concentration of the doped Ag nanoparticles, the absorption of the analytical solution to the spectrum is gradually increased, reaching up to the maximum value of 0.05 mol/L $AgNO_3$ solution. The change regulation of the dye adsorption amount is also the same. Table 1 shows the dye adsorption amount of different concentration of the Ag-doped TNT arrays composite film

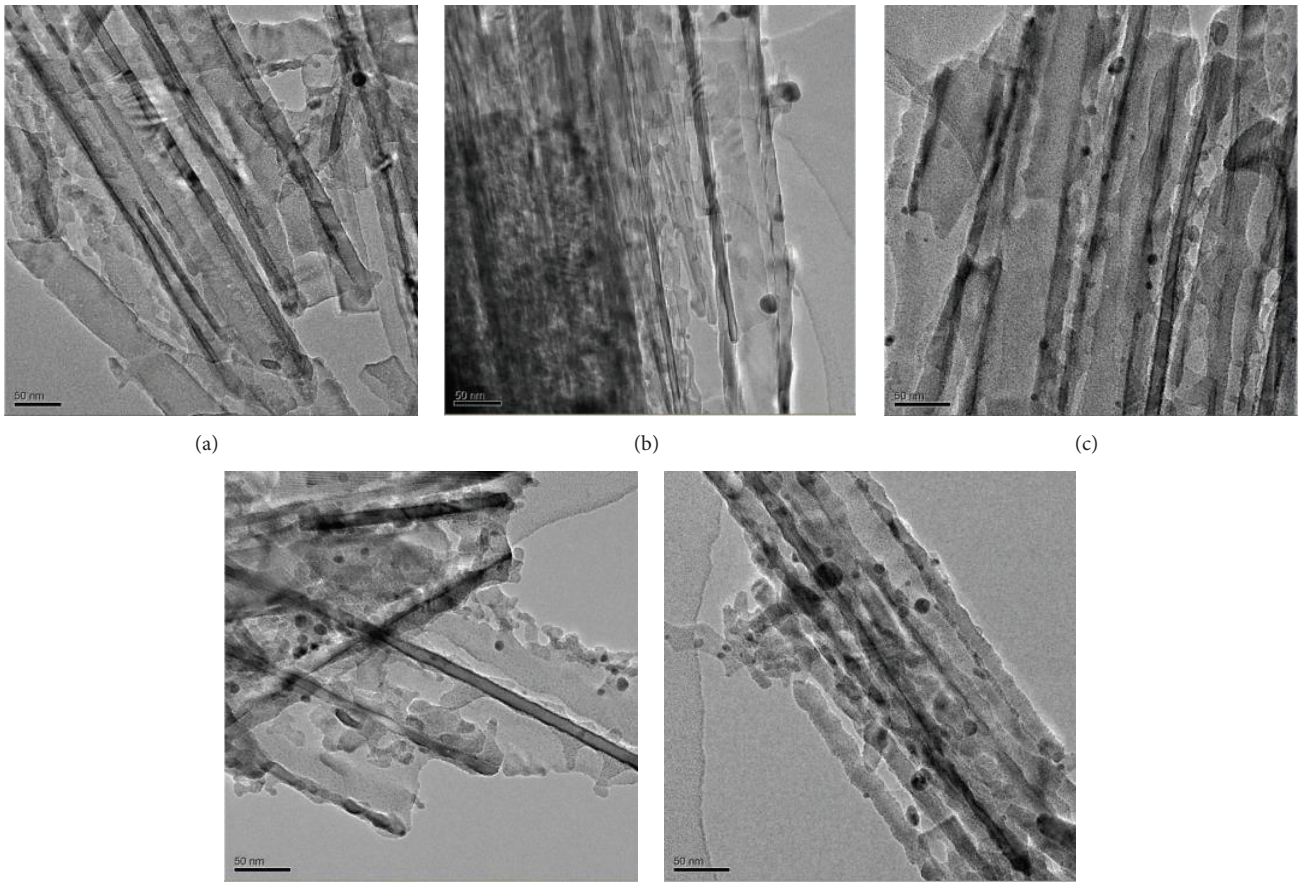

Figure 4: The TEM images of the different concentration Ag-doped TNT arrays. 0.01 mol/L $AgNO_3$ (a), 0.02 mol/L $AgNO_3$ (b), 0.03 mol/L $AgNO_3$ (c), 0.04 mol/L $AgNO_3$ (d), and 0.05 mol/L $AgNO_3$ (e).

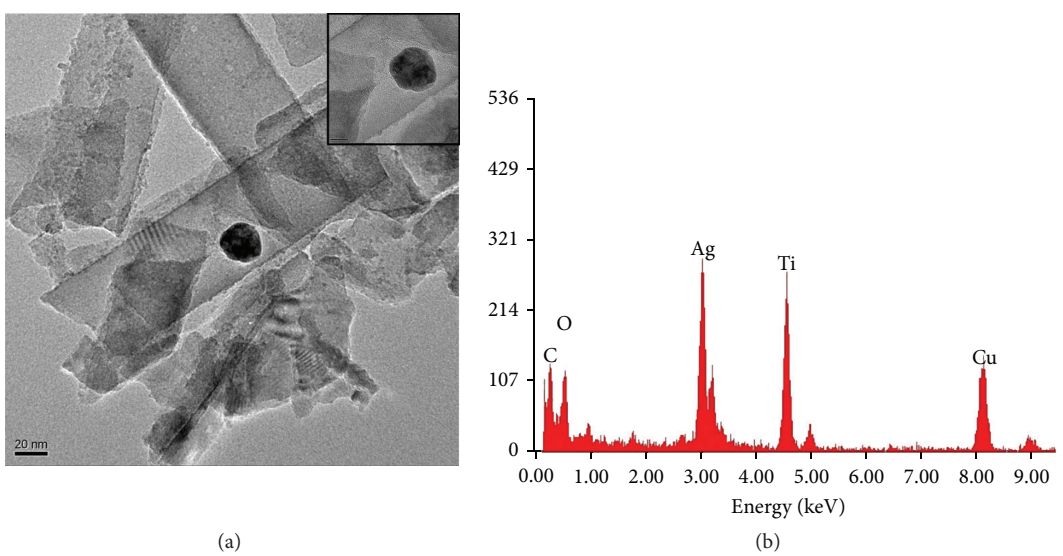

Figure 5: The TEM images of a single Ag-doped TiO_2 nanotube (a), the energy spectrum of the black point in (a) picture (b).

Table 1: The dye adsorption amount of different concentration of the Ag-doped TNT arrays composite film photoanode.

Sample ($AgNO_3$ mol/L)	NO (Ag)	0.01	0.02	0.03	0.04	0.05
Absorbed dye amount ($\times 10^{-7}$ mol/cm^2)	2.22	3.52	3.69	4.35	4.74	4.93

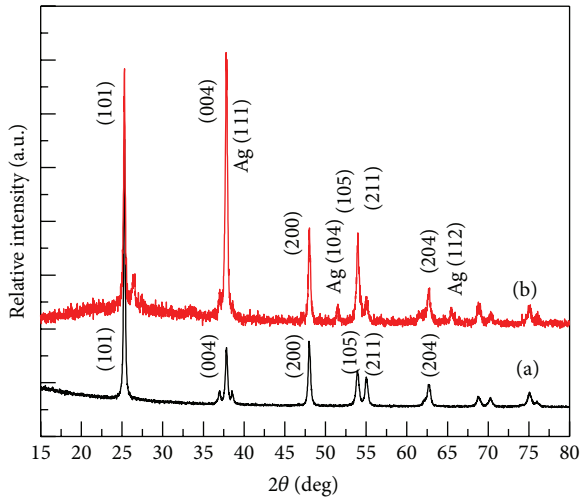

(a) TNT arrays
(b) Ag + TNT arrays

Figure 6: The XRD patterns of TNT arrays composite film photoanode. TNT arrays composite film (a) and the Ag-doped TNT arrays composite film photoanode.

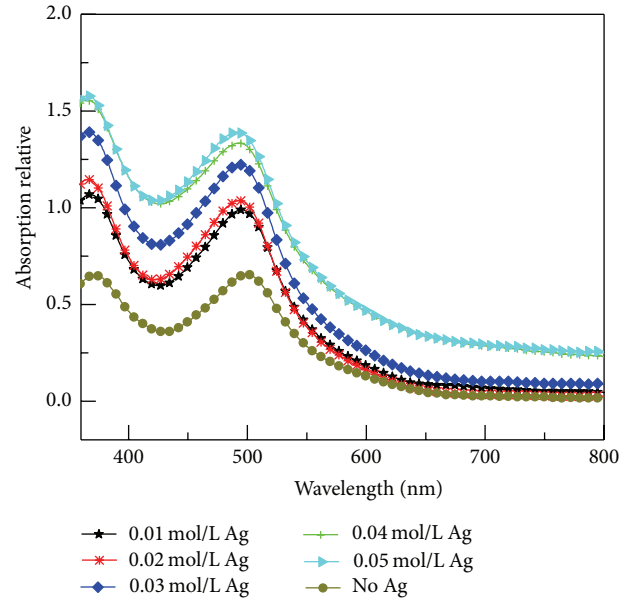

Figure 7: The spectral absorption of analytical solution of different concentration of the Ag-doped TNT arrays composite film photoanode.

photoanode. The main reason for that was that the metal bond between the Ag nanoparticles formed many metal clusters. These clusters have large surface area, which can greatly improve the dye adsorption and enhance the photoelectric conversion efficiency of the DSSCs.

Figure 8 shows the UV-Vis absorption spectra of the Ag-doped TNT arrays composite film photoanode. It can be seen clearly that the absorption performance of the Ag-doped TNT arrays composite photoanode has a great improvement in the UV-Vis spectral range especially in the range of the 400–800 nm, compared to the pure TNT arrays composite film photoanode. In general, with the increase of the doping concentration, the absorption capacity of the light spectra is also enhanced, reaching up to the maximum value in 0.04 mol/L $AgNO_3$ solution. Continuing to increase concentration, the absorption capacity of the light spectra will be reduced. The main reason for this phenomenon may be that when the TNT arrays film is exposed to sunlight, the interaction between the free electron on the surface of Ag nanoparticles and the photons makes the Surface Plasmon Resonance Effect on the TNT arrays film. And the resonance greatly improves the photocatalytic performance of the TNT arrays film photoanode [30, 31]. The reason for the decrease of the spectra absorption capacity may be that more Ag nanoparticles hinder the transmission of electrons, reduce the transmission rate of the electron, and suppress the interaction between electrons and photons.

3.4. Photovoltaic Performance of DSSCs. The current density-voltage (J-V) curve of DSSCs based on the different concentration Ag-doped TNT arrays composite film photoanode was shown in Figure 9. And the detailed photoelectric performance parameters such as open circuit voltage (V_{OC}), short circuit current density (J_{SC}), fill factor (FF), and the photoelectric conversion efficiency are obtained and shown in Table 2. It displays that the Ag-doped TNT arrays composite film photoelectrodes showed a higher efficiency of 6.12% compared to the pure TNT arrays composite film photoelectrodes of 3.00%. The increase is mainly manifested in the improvement of the short circuit current density (J_{SC}) from the no Ag-doped photoelectrode of 9.65 mA/cm^2 up to the Ag-doped photoelectrode of 14.53 mA/cm^2. What is more, with the increase of the doping concentration, the photoelectric conversion efficiency is gradually improved, reaching up to the maximum in the 0.04 mol/L $AgNO_3$ solution, which is slightly decreased to 5.43% after continuing to increase the doping concentration. This result is in agreement with the UV-Vis absorption spectra test, which may be because of the following reasons: (1) the clusters of the Ag nanoparticles have large surface area, which show great performance of the dye adsorption. (2) When the Ag nanoparticles were doped into the TNT arrays film, the interaction of the free electron on the Ag nanoparticles and the photons produces the Surface Plasmon Resonance Effect on the TNT arrays film, which greatly improved the

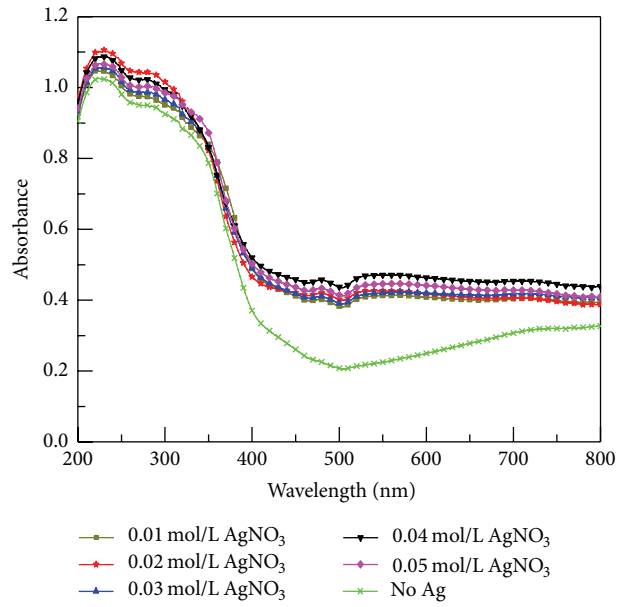

Figure 8: The UV-Vis absorption spectra of the Ag-doped TNT arrays composite.

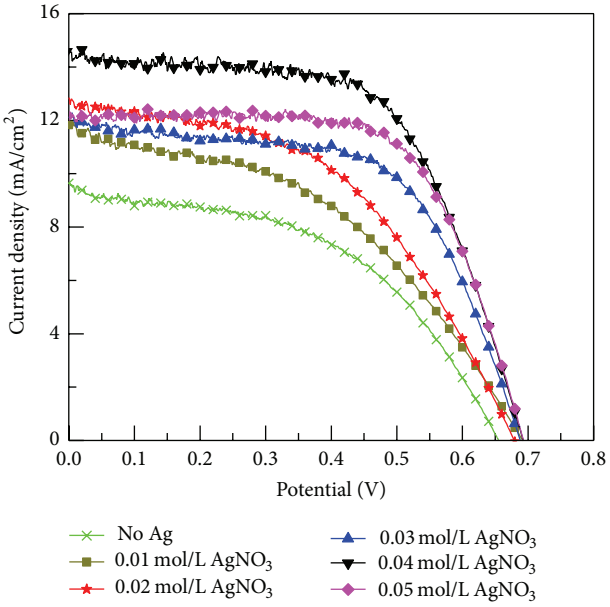

Figure 9: The current density-voltage (J-V) curve of DSSCs based on the different concentration Ag-doped TNT arrays composite film photoanode.

photocatalytic ability and spectral response range of the TNT arrays composite film photoelectrode. However, too much Ag nanoparticles will hinder the transmission of electrons, reduce the transmission rate of the electron, and suppress the interaction between electrons and photons.

4. Conclusions

In conclusion, we successfully fabricated the five different concentrations of the Ag-doped TNT arrays composite film photoelectrode and compared them to the pure TNT arrays composite film in the XRD pattern, microstructure, UV-Vis absorption spectra, and photovoltaic performance. The XRD pattern confirms that the pure TNT arrays film and the photoelectrode after doping Ag nanoparticles are both of anatase phase structure. The microstructure measurement proved the existence of the Ag nanoparticles and showed the cluster structure of it. The UV-Vis absorption spectra illustrate that the cluster structure has large surface area that contributes to dye adsorption and the Surface Plasmon Resonance Effect of the Ag nanoparticles improved the photocatalytic ability of the TNT arrays film, but too much Ag nanoparticles suppressed the interaction between electrons and photons so as to reduce the capacity of light absorption. With the increase of the doping concentration, the efficiency of the TNT arrays composite film electrode has the trend of first rising and then falling, from 3.00% of the pure TNT arrays composite photoanode to 6.12% of the Ag-doped TNT arrays photoanode and then down to 5.43%; the maximum is in the 0.04 mol/L $AgNO_3$ solution. The improvement of efficiency was mainly due to the strong dye adsorption capacity of the cluster and the photocatalytic ability of the Ag nanoparticles.

Table 2: Comparison of the photovoltaic performances of the different concentration Ag-doped TNT arrays composite film photoanode.

$AgNO_3$ (moL/L)	V_{OC} (V)	J_{SC} (mA/cm^2)	FF	η
NO Ag	0.655	9.65	0.47	3.00%
0.01	0.691	11.82	0.44	3.56%
0.02	0.679	12.85	0.48	4.15%
0.03	0.688	12.1	0.59	4.93%
0.04	0.692	14.53	0.61	6.12%
0.05	0.693	12.12	0.65	5.43%

Competing Interests

The authors declare that they have no competing interests.

Authors' Contributions

Jinghua Hu and Jiejie Cheng contributed equally to this work.

Acknowledgments

This work was supported by the NSFC (51572072 and 11204070) and the Fundamental Research Funds for the Central Universities (2014-Ia-028). This work was also financially supported by State Key Laboratory of Advanced Technology for Materials Synthesis and Processing (2016-KF-13).

References

[1] B. O'Regan and M. Grätzel, "A low-cost, high-efficiency solar cell based on dye-sensitized colloidal TiO_2 films," *Nature*, vol. 353, no. 6346, pp. 737–740, 1991.

[2] M. Grätzel, "Photoelectrochemical cells," *Nature*, vol. 414, no. 6861, pp. 338–344, 2001.

[3] J. Sheng, L. Hu, S. Xu et al., "Characteristics of dye-sensitized solar cells based on the TiO_2 nanotube/nanoparticle composite electrodes," *Journal of Materials Chemistry*, vol. 21, no. 14, pp. 5457–5463, 2011.

[4] J. van de Lagemaat, N.-G. Park, and A. J. Frank, "Influence of electrical potential distribution, charge transport, and recombination on the photopotential and photocurrent conversion efficiency of dye-sensitized nanocrystalline TiO_2 solar cells: a study by electrical impedance and optical modulation techniques," *The Journal of Physical Chemistry B*, vol. 104, no. 9, pp. 2044–2052, 2000.

[5] J. Hu, L. Zhao, Y. Yang et al., "TiO_2 nanotube arrays composite film as photoanode for high-efficiency dye-sensitized solar cell," *International Journal of Photoenergy*, vol. 2014, Article ID 602692, 8 pages, 2014.

[6] W.-Q. Wu, Y.-F. Xu, H.-S. Rao, C.-Y. Su, and D.-B. Kuang, "A double layered TiO_2 photoanode consisting of hierarchical flowers and nanoparticles for high-efficiency dye-sensitized solar cells," *Nanoscale*, vol. 5, no. 10, pp. 4362–4369, 2013.

[7] J. Liu, A. X. Wei, Y. Zhao, K. B. Lin, and F. Z. Luo, "Dye-sensitized solar cells based on ZnO nanoflowers and TiO_2 nanoparticles composite photoanodes," *Journal of Materials Science: Materials in Electronics*, vol. 25, no. 2, pp. 1122–1126, 2014.

[8] A. C. Fisher, L. M. Peter, E. A. Ponomarev, A. B. Walker, and K. G. U. Wijayantha, "Intensity dependence of the back reaction and transport of electrons in dye-sensitized nanocrystalline TiO_2 solar cells," *The Journal of Physical Chemistry B*, vol. 104, no. 5, pp. 949–958, 2000.

[9] M. Law, L. E. Greene, J. C. Johnson, R. Saykally, and P. Yang, "Nanowire dye-sensitized solar cells," *Nature Materials*, vol. 4, no. 6, pp. 455–459, 2005.

[10] P. E. de Jongh and D. Vanmaekelbergh, "Trap-limited electronic transport in assemblies of nanometer-size TiO_2 particles," *Physical Review Letters*, vol. 77, no. 16, pp. 3427–3430, 1996.

[11] W.-Y. Rho, H. Jeon, H.-S. Kim, W.-J. Chung, J. S. Suh, and B.-H. Jun, "Recent progress in dye-sensitized solar cells for improving efficiency: TiO_2 nanotube arrays in active layer," *Journal of Nanomaterials*, vol. 2015, Article ID 247689, 17 pages, 2015.

[12] X. J. Feng, K. Shankar, O. K. Varghese, M. Paulose, T. J. Latempa, and C. A. Grimes, "Vertically aligned single crystal TiO_2 nanowire arrays grown directly on transparent conducting oxide coated glass: synthesis details and applications," *Nano Letters*, vol. 8, no. 11, pp. 3781–3786, 2008.

[13] B. Liu and E. S. Aydil, "Growth of oriented single-crystalline rutile TiO_2 nanorods on transparent conducting substrates for dye-sensitized solar cells," *Journal of the American Chemical Society*, vol. 131, no. 11, pp. 3985–3990, 2009.

[14] T. Yuan, H. B. Lu, B. H. Dong et al., "Single-crystalline rutile TiO_2 nanorod arrays with high surface area for enhanced conversion efficiency in dye-sensitized solar cells," *Journal of Materials Science: Materials in Electronics*, vol. 26, no. 3, pp. 1332–1337, 2015.

[15] M. Adachi, Y. Murata, I. Okada, and S. Yoshikawa, "Formation of titania nanotubes and applications for dye-sensitized solar cells," *Journal of the Electrochemical Society*, vol. 150, no. 8, pp. G488–G493, 2003.

[16] L. Zhao, J. G. Yu, J. J. Fan, P. C. Zhai, and S. M. Wang, "Dye-sensitized solar cells based on ordered titanate nanotube films fabricated by electrophoretic deposition method," *Electrochemistry Communications*, vol. 11, no. 10, pp. 2052–2055, 2009.

[17] K. Asagoe, S. Ngamsinlapasathian, Y. Suzuki, and S. Yoshikawa, "Addition of TiO_2 nanowires in different polymorphs for dye-sensitized solar cells," *Central European Journal of Chemistry*, vol. 5, no. 2, pp. 605–619, 2007.

[18] M. Adachi, Y. Murata, J. Takao, J. Jiu, M. Sakamoto, and F. Wang, "Highly efficient dye-sensitized solar cells with a titania thin-film electrode composed of a network structure of single-crystal-like TiO_2 nanowires made by the 'oriented attachment' mechanism," *Journal of the American Chemical Society*, vol. 126, no. 45, pp. 14943–14949, 2004.

[19] J. T. Jiu, S. J. Isoda, F. M. Wang, and M. Adachi, "Dye-sensitized solar cells based on a single-crystalline TiO_2 nanorod film," *The Journal of Physical Chemistry B*, vol. 110, no. 5, pp. 2087–2092, 2006.

[20] H. Hafez, Z. Lan, Q. Li, and J. Wu, "High efficiency dye-sensitized solar cell based on novel TiO_2 nanorod/nanoparticle bilayer electrode," *Nanotechnology, Science and Applications*, vol. 3, no. 1, pp. 45–51, 2010.

[21] C. Rho and J. S. Suh, "Filling TiO_2 nanoparticles in the channels of TiO_2 nanotube membranes to enhance the efficiency of dye-sensitized solar cells," *Chemical Physics Letters*, vol. 513, no. 1–3, pp. 108–111, 2011.

[22] J. Hu, J. Cheng, S. Tong, L. Zhao, J. Duan, and Y. Yang, "Dye-sensitized solar cells based on P25 nanoparticles/TiO_2 nanotube arrays/hollow TiO_2 boxes three-layer composite film," *Journal of Materials Science: Materials in Electronics*, vol. 27, no. 5, pp. 5362–5370, 2016.

[23] C. Photiphitak, P. Rakkwamsuk, P. Muthitamongkol, and C. Thanachayanont, "A combined effect of plasmon energy transfer and recombination barrier in a novel TiO_2/MgO/Ag working electrode for dye-sensitized solar cells," *International Journal of Photoenergy*, vol. 2015, Article ID 795138, 10 pages, 2015.

[24] J. Wang, Y. Xie, Z. Zhang et al., "Application of TiO_2/Er^{3+}:$Y_3Al_5O_{12}$ composite to photo-degrade acid red B dye under sun light irradiation," *Russian Journal of Physical Chemistry A*, vol. 83, no. 13, pp. 2350–2356, 2009.

[25] L. Q. Wang, L. S. Jia, and Q. B. Li, "A novel sulfur source for biosynthesis of (Ag, S)-modified TiO_2 photoanodes in DSSC," *Materials Letters*, vol. 123, no. 9, pp. 83–86, 2014.

[26] S. D. Standridge, G. C. Schatz, and J. T. Hupp, "Distance dependence of plasmon-enhanced photocurrent in dye-sensitized solar cells," *Journal of the American Chemical Society*, vol. 131, no. 24, pp. 8407–8409, 2009.

[27] M. D. Brown, T. Suteewong, R. S. S. Kumar et al., "Plasmonic dye-sensitized solar cells using core-shell metal-insulator nanoparticles," *Nano Letters*, vol. 11, no. 2, pp. 438–445, 2011.

[28] J. Qi, X. Dang, P. T. Hammond, and A. M. Belcher, "Highly efficient plasmon-enhanced dye-sensitized solar cells through metal@oxide core-shell nanostructure," *ACS Nano*, vol. 5, no. 9, pp. 7108–7116, 2011.

[29] N.-G. Park, G. Schlichthörl, J. van de Lagemaat, H. M. Cheong, A. Mascarenhas, and A. J. Frank, "Dye-sensitized TiO_2 solar cells: structural and photoelectrochemical characterization of nanocrystalline electrodes formed from the hydrolysis of $TiCl_4$," *The Journal of Physical Chemistry B*, vol. 103, no. 17, pp. 3308–3314, 1999.

[30] N. Pugazhenthiran, S. Murugesan, and S. Anandan, "High surface area Ag-TiO_2 nanotubes for solar/visible-light photocatalytic degradation of ceftiofur sodium," *Journal of Hazardous Materials*, vol. 263, no. 2, pp. 541–549, 2013.

[31] W.-Y. Rho, H.-S. Kim, S. H. Lee et al., "Front-illuminated dye-sensitized solar cells with Ag nanoparticle-functionalized freestanding TiO_2 nanotube arrays," *Chemical Physics Letters*, vol. 614, pp. 78–81, 2014.